

An approach for performance prediction of saturated brushed permanent magnet direct current (DC) motor from physical dimensions

Rasul Tarvirdilu–Asl¹ , Reza Zeinali² , Hulusi Bulent Ertan^{3,*} 

¹Canada Excellence Center, McMaster University, Ontario, Canada

²Department of Electrical Engineering, Eindhoven University of Technology, Eindhoven, The Netherlands

³Mechatronics Engineering Department, Atılım University, Ankara, Turkey

Received: 04.08.2020

Accepted/Published Online: 20.01.2021

Final Version: 19.01.2022

Abstract: An analytical approach for performance prediction of saturated brushed permanent magnet direct current (DC) motors is proposed in this paper. In case of a heavy saturation in the stator back core of electrical machines, some flux completes its path through the surrounding air, and the conventional equivalent circuit cannot be used anymore. This issue has not been addressed in the literature. The importance of considering the effect of the flux penetrating the surrounding air is shown in this paper using finite element simulations and experimental results, and an analytical approach is proposed to consider this effect on magnet operating point determination and performance prediction of saturated brushed permanent magnet DC motors. An analytical method is also presented to determine the boundary radius of the surrounding air for obtaining accurate results in finite element (FE) solutions and analytical calculations. An analytical approach based on Carter's coefficient is also proposed to calculate the effective length of the magnet when the length of the magnet and rotor length are not the same. The accuracy of the proposed analytical model is illustrated using finite element simulations and experimental results. With this accuracy, this analytical model is very suitable to be used for reliable and quick mathematical design optimization.

Key words: Analytical modeling, finite element simulations, magnet operating point, permanent magnet brushed DC motor

1. Introduction

Despite the great competition from other types of motors such as switched reluctance and brushless permanent magnet motors, brushed permanent magnet direct current (DC) motors are still dominant in low power and cost-sensitive applications. These motors are used in many automotive applications, including electro-hydraulic systems [1]. Cheaper production cost and lower fabrication time are some of the advantages offered by permanent magnet direct current (PMDC) motors with brushes. DC machines with wound field windings are also popular in the industry. Weight optimization of brush-type DC machines with wound field excitation is aimed at [2] and [3]. However, permanent magnet excitation is dominant for the reasons discussed in [4]. With the availability of cheaper permanent magnets, the wound field in DC machines is often replaced with permanent magnets, making this type of motor very popular in many applications. As a consequence, although their design methodology is well studied, there is still considerable research on this type of motor [4–6, 12]. Accurate analysis and design optimization are naturally of much interest.

*Correspondence: bulent.ertan@atilim.edu.tr

Finite element method (FEM) is implemented in lots of research conducted on design, weight, and cost optimizations of electrical machines [7–10]. The design of PM machines using the finite element method is aimed at [11]. A significant reduction in weight and volume of the motor is attained using the finite element method in [13], based on using a new magnetic material. FEM-based geometry modifications are proposed in [13] to reduce acoustic noise and cogging torque in a brushed PMDC motor, to be used in the automotive cooling system application. However, using a pure FEM-based study can be tedious and time-consuming due to the huge number of iterations required in solving the optimization problem. On the other hand, a precise analytical model can give a thorough insight into the problem and reduce the optimization time greatly.

Combining FEM and analytical model can also be utilized for design optimization purposes, which merges the accuracy of the finite element method with the rapidity of analytical calculations [9]. In some cases, analytical models can be improved by employing finite element method results or measurements [14, 15]. Flux and flux density distribution and motor parameters including winding inductances can be computed using FEM, and used in analytical models to predict motor performance using analytical equations [16].

An accurate analytical model of a DC motor can be used for performance calculation, current control [17], speed control [18–21], and for design and optimization purposes [14]. Determination of the air gap flux is an important task. A linear magnetic circuit is assumed in some studies [22–24], which reduces the complexity of taking nonlinearities into account. However, the accuracy of the obtained solution will be low in such an approach. Some other methods have also been proposed in the literature to calculate the magnetic flux distribution. For example, in [25], analytic magnetic field solution is obtained with certain simplifying assumptions, by solving Laplacian/quasi–Poissonian magnetic field equations to determine the magnetic flux distribution in the air gap region of a permanent magnet brushed DC motor. In another study, Maxwell equations in two-dimensional space are used to develop an analytical model for the determination of no-load flux in a brushed PMDC motor [15].

Avoiding magnetic saturation in core material may be a crucial step in improving the performance of electrical machines; however, it may not be always possible due to manufacturing constraints. It is noticeable that, in heavy saturation conditions, some flux completes its path through the surrounding air instead of the motor’s magnetic circuit, and the general magnetic equivalent circuit cannot be used to calculate DC motor performance. This issue is discussed by several authors in the literature [26–28]. The papers mentioned above do not take into account the effect of the flux which leaks out of the stator frame and completes its path through the surrounding air. However, an accurate analytical model which considers saturation effects can accelerate the design calculations and offers a very handy tool to design engineers.

The difference in magnet, stator, and rotor lengths in PM brushed DC motors increases the complexity of analytical modeling and calculations of the machine, because, in the determination of the magnet operating point, effective magnet length has to be taken into account. [29] investigates the effects of magnet length in AC machines. In this paper, we also present an analytical solution to this problem.

The main contributions of this paper are summarized as follows; first, an analytical approach is proposed to consider the effect of the flux completing its path through the surrounding air in magnet operating point determination and performance prediction of saturated brushed PMDC motors. This approach can be further generalized to be used for any saturated electric machine. Second, an analytical method is developed to estimate the boundary radius of the surrounding air for obtaining accurate results in FE solutions and analytical calculations.

In this paper, in section 2, the steady-state equivalent circuit, calculation of induced emf, and armature

resistance of a PM brushed DC motor and prediction of its steady-state performance are discussed. Section 3 involves the calculation of the magnet operating point while taking into account the effective length of the magnet (due to the difference between magnet and rotor axial lengths) and the flux leaking to the surrounding air under heavy saturation conditions. A method is also proposed to determine the magnetomotive force (MMF) drop on the stator back core for this case. Finally, in Sections 4 and 5, analytically calculated results are compared with measurements and finite element simulation results of a test PMDC motor to verify the accuracy of the proposed analytical methods.

2. Prediction of steady-state performance

The circuit model for prediction of the steady-state performance of a brushed DC motor is well established. This model requires the induced armature electromotive force (emf) and the armature resistance values for predicting the motor speed and efficiency at a certain terminal voltage. Therefore, at the design stage, the problem is that of calculation of armature resistance and the induced emf on the armature windings at a given speed, using the information available for the geometry of the magnetic circuit and material properties. It is known that the induced emf, E_a , can be calculated from equation (1).

$$E_a = k\varphi_p\omega_m = \frac{pZ_a}{2\pi a} \times B_{av} \times \frac{\pi D_i}{p} \times L \times \omega_m \quad (1)$$

where, k is the motor constant. φ_p and ω_m are the pole flux in Wb and mechanical speed in rad/sec respectively. Pole number of the PMDC motor is shown by p . Z_a , a , B_{av} , and D_i are the number of conductors of armature winding, number of parallel paths in the winding, air gap mean flux density, and inner diameter of the stator, respectively. L stands for rotor core axial length.

The armature resistance calculation from the physical dimensions is quite straightforward. The cross-section of a typical PM brushed DC motor is shown in Figure 1a. Suppose that there are S_a slots on the armature and each slot has Z_{as} conductors, and there are “a” parallel paths.

Assuming that the dimensions of the motor and the wire material are known, the resistance of one of the paralleled coils can be calculated using equation (2).

$$R_{coil} = \rho \frac{L_{coil}}{A_{wire}} = \rho \frac{N_{coil} \times 2 \times (L + L_{end}) + L_{wc}}{\frac{\pi d_c^2}{4}} \quad (2)$$

In this equation, the copper resistivity is shown by ρ . L_{coil} , A_{wire} , and N_{coil} are total length of wire in one coil, wire cross-sectional area, and number of turns per coil, respectively. L_{end} is the end winding length, which also includes coil end extension, and d_c is the wire diameter. L_{wc} stands for coil to commutator bar connection (see Figure 1b). The resistance seen at the armature terminals is as given in equation (3)

$$R_a = R_{brush} + \frac{N_{active}R_{coil}}{a} \quad (3)$$

where a is the number of parallel paths and N_{active} is the number of active coils taking into account the coils shorted by the brushes. R_{brush} stands for the brush resistance.

The difficulty in establishing the equivalent circuit of a given motor stems from the difficulty associated with predicting the value of induced armature emf. More precisely, from the difficulty of calculating flux per

pole accurately for a given magnet shape and taking saturation into account in the magnetic circuit, in case it exists. The following section addresses this problem and introduces a new approach for accurate calculation of the pole flux.

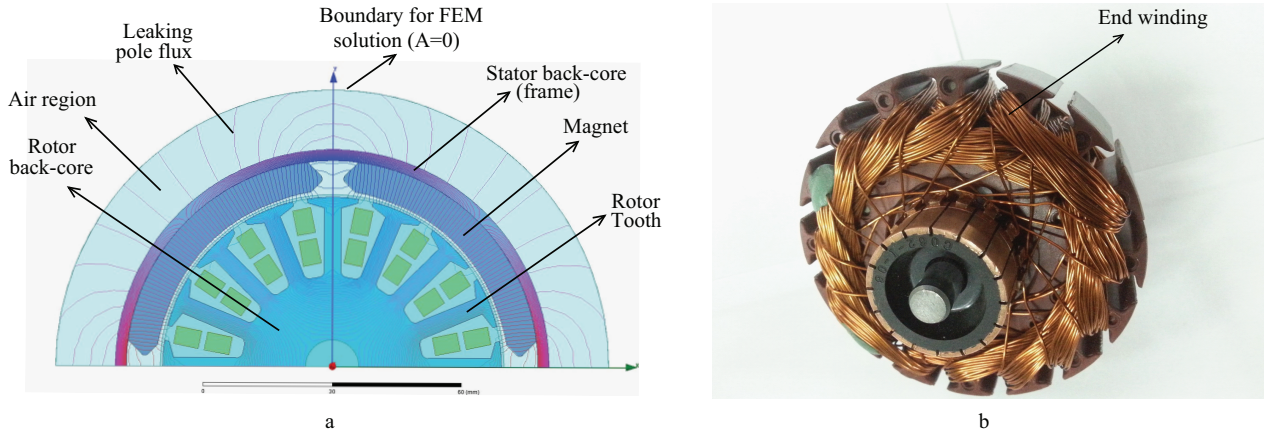


Figure 1. (a) Cross section of the test motor and flux leaking to the surrounding air. (b) Rotor and winding configuration of the test motor.

3. Calculation of flux per pole

Most commercial motors have some saturation in their magnetic circuit. Unless this is taken into account, the induced emf cannot be well predicted, and the performance of the motor cannot be accurately determined. A further difficulty arises if the magnet axial length and the core length are not identical (see Figure 2).

3.1. Effective axial length of magnet

As shown in Figure 2 the magnet axial length may not be the same as rotor core axial length.

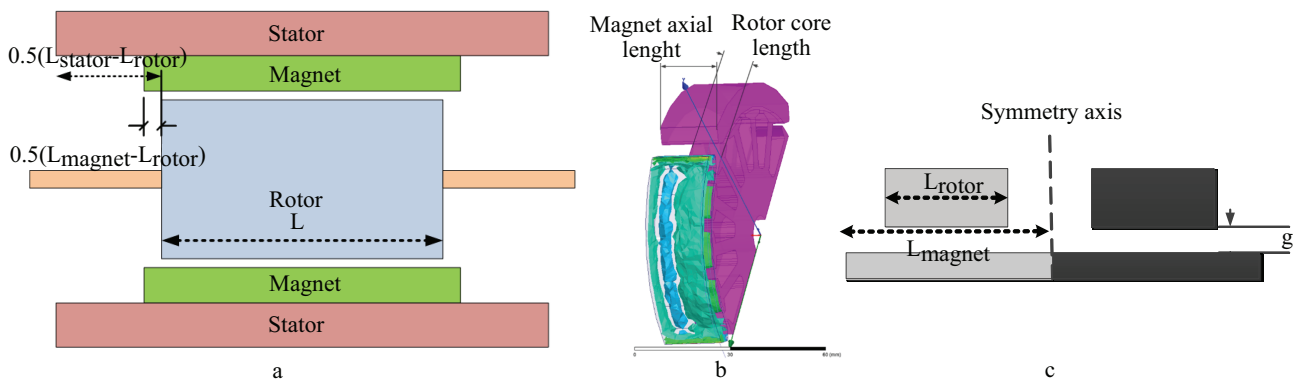


Figure 2. (a) Cross section of the test motor and flux leaking to the surrounding air. (b) Rotor and winding configuration of the test motor. (c) Motor and its mirror image (axial view) for calculation of effective core length using Carter's coefficient.

The calculation of pole flux created by the magnet depends on what the effective axial length of the magnet is. Magnetic flux density distribution inside the magnet obtained using 3-D finite element simulations is shown in Figure 2b. It is observed that the flux density distribution inside the magnet is not uniform and

the flux density is reduced towards the magnet edges in the axial direction. Therefore, an effective length of the magnet needs to be defined.

To estimate the effective axial length of the magnet, the model shown in Figure 2c is used. This model is created by placing mirror image of the axial view of a PM motor (The mirror image is distinguished by its darker colour in this figure). Considering the geometry in Figure 2c, Carter’s coefficient (c_s) can be calculated from equation (4) [30, 31]. The effective length of the magnet can then be calculated by dividing the magnet length of the PMDC motor to the calculated Carter’s coefficient.

$$C_s = \frac{L_{\text{magnet}}}{L_{\text{rotor}} + \frac{4g}{\pi} \ln \left(1 + \frac{\pi(L_{\text{magnet}} - L_{\text{rotor}})}{4g} \right)} \quad (4)$$

The accuracy of this approach is very good, as can be followed from Table 1, where the analytically calculated air gap flux density and FE results are given for a test motor (both with and without outer air region), using the approach described above. This table also compares FEM obtained values with the analytically calculated rotor tooth flux density and stator back core flux density, under open circuit condition. The error between the analytical calculation and FEM calculations are also presented in the table. Column 3 is the error between FEM and analytical calculation without the outer air region. Column 6 presents the error between analytical and FEM predictions when the outer air region is considered. Finally, the last column presents the error in FEM calculations with and without considering the outer region. This last column indicates that when the outer air region flux is considerable, it needs to be included in the predictions for good accuracy. The analytical air gap flux density calculation procedure is explained in section 3.2.

Table 1. Analytically calculated flux density levels calculated using Carter’s coefficient and FEM simulations results (with and without considering the outer air region)

	Without considering the outer air region			Considering the outer air region		Difference between FE results with and without considering the outer air region (%)	
	Analytical	FEM	Error (%)	Analytical	FEM	With outer air region Error between analytic and FEM (%)	Error between FEM with and without outer air region (%)
Magnet flux density (mean)	0.27	0.266	1.5	0.284	0.278	2.16	4.5
Air gap flux density (mean)	0.29	0.281	3.2	0.31	0.303	2.31	7.8
Tooth flux density (mean)	1.46	1.4	4.2	1.55	1.58	1.9	12.9
Stator back-core flux density (peak)	2.35	2.37	0.84	2.25	2.20	2.27	7.2

3.2. Calculation of magnet operating point

For the calculation of the open circuit induced emf on the armature winding, the only unknown parameter in equation (1) is the mean flux density in the air gap (B_{av}). To determine B_{av} , the operating point of the magnet must be found. The magnet operating point is defined as the intersection point of magnet recoil line and load

line. To determine the intersection point, load line and magnet recoil line equations have to be determined. In developing the load line equation, MMF drop on the rotor back-core is often negligible, if not, this can be taken into account using a similar procedure that used here in Section 3.2.1.

3.2.1. Calculation of load line

Load line calculation involves estimating the MMF expended on the magnetic circuit for a certain magnet flux density (B_m). For a given B_m , flux per pole is ($\varphi_m = B_m A_m$), where A_m is the effective magnet area under a pole pitch. The MMF required to force φ_m can be calculated by applying Ampere's law. Armature reaction is neglected in determination of magnet operating point in the proposed analytical model in this paper. Consider a closed loop which crosses the air gap at points a pole pitch apart as shown in Figure 4a. Assuming that, with the exception of stator back iron and rotor teeth, the magnetic circuit is infinitely permeable, equation (5) can be written under no-load condition.

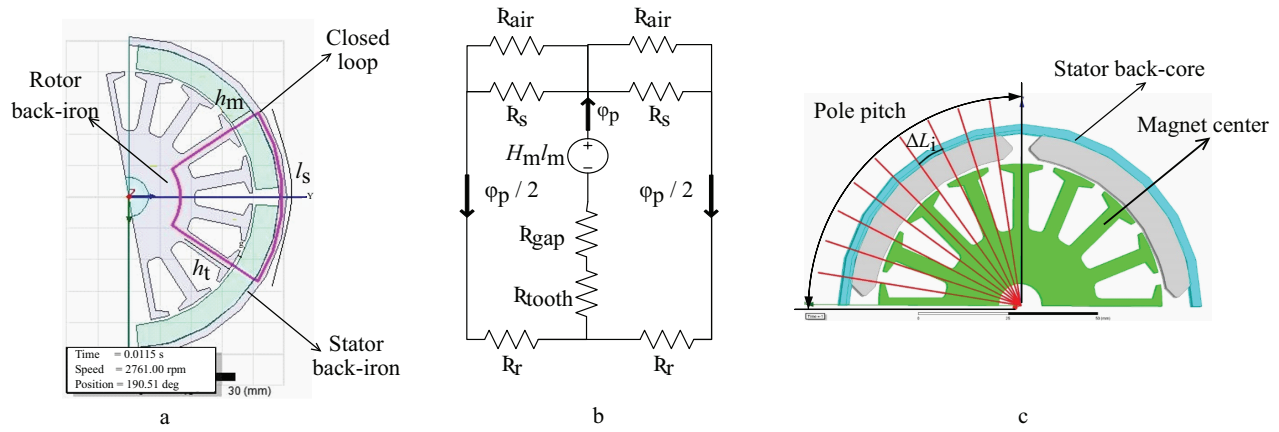


Figure 3. (a) The closed loop to write load line equation. (b) Magnetic equivalent circuit. (c) Division of stator back core into ten equal sections.

$$f = 2H_m h_m + 2H_g g + 2H_t h_t + H_s l_s = 0 \quad (5)$$

Where, H is the field intensity in related region; h_m , g , h_t and l_s stand for magnet height, air gap length, rotor tooth height and stator back iron flux path length, respectively. Therefore, the operating point of the magnet can be found by determining the values of the field intensity in the sections of the magnetic circuit considered in equation (5). In the design here, a ferrite magnet is used. The magnet characteristic is linear and is approximated by equation (6).

$$B_m = \frac{0.405}{298334.1} (H_m + 298334.1) \quad (6)$$

The obstacle in this calculation is the calculation of the flux leaking out from the frame into the air if the stator back core is saturated. This phenomenon is shown in Figure 1a. The flux density levels for different parts of the PMDC motor shown in this figure are given in Table 1. Note that, when the flux leaks out of the core, the classical magnetic circuit of the motor [32] needs to be modified by adding shunt reluctances to the

flux paths of the flux in the stator back iron. The modified equivalent magnetic circuit is depicted in Figure 3b. In this figure reluctance $\mathfrak{R}_{\text{air}}$ represents the air region reluctance outside the stator, through which leakage flux flows. Estimation of the value of the leakage flux path reluctance is discussed in the following section.

3.2.2. Calculation of stator back core flux density considering the flux leaking out from the frame

The algorithm for the calculation of core flux density and MMF expended on this part of the magnetic circuit is developed by studying the problem on the test motor described in Section 4. The problem is studied via 3-D FEM simulations. In such FEM solutions, the flux is usually assumed to be confined to the core and $A = 0$ is assigned to the boundary of the frame. Obviously, this would lead to erroneous results if the flux is leaking out of the frame. Therefore, in studying the frame, $A = 0$ is assigned to the outer boundary of the air region surrounding the stator (Figure 1). The choice of the location of this boundary is discussed in Appendix A. When the FEM results are studied it is found out that except the stator back core, the magnetic circuit remains unsaturated. The solution also reveals that some of the pole flux completes its path through the air (Figure 1a). The solutions also display how the flux density is distributed in the back core. This is shown in Figure 4a. It is observed that stator back-core flux density reaches its minimum at the location corresponding to the center of the pole magnet (see Figure 4 and Figure 3). The stator back core flux density maximum is at the point between two adjacent magnets. So, in order to calculate the MMF drop on stator back-core analytically, this path (with a length equal to pole pitch) is divided into 10 equal sections as seen in Figure 3c.

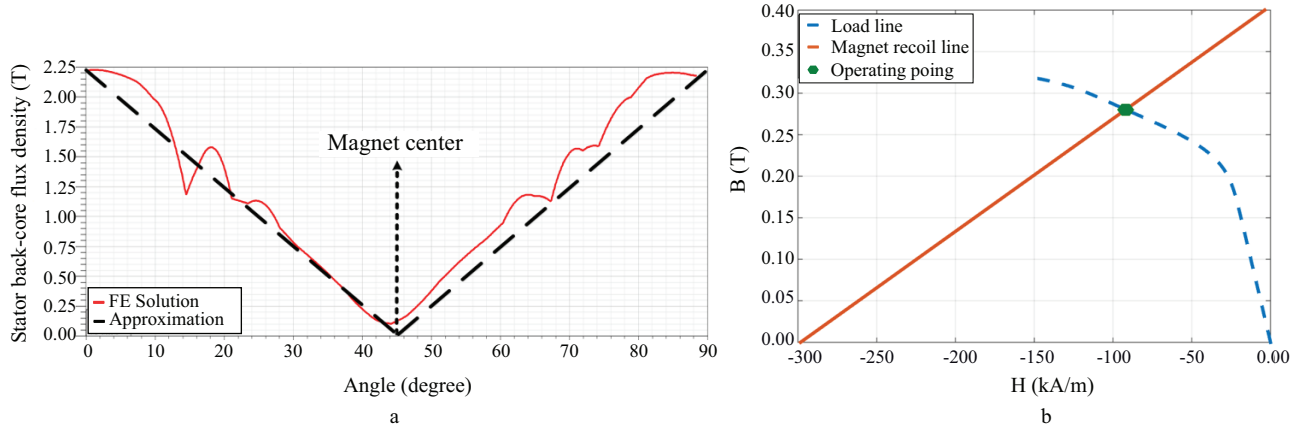


Figure 4. (a) Stator back-core flux density variation of the test machine under a pole. Solid line (red): FEM solution, dashed black line: linear approximation). (b) Test motor magnet recoil line and load line.

For the 4-pole test motor here ($pole\ pitch = 90^\circ$) with magnet span of 81° , the stator back core flux density reaches its maximum value at $45^\circ + (81^\circ/2) = 85.5^\circ$, and is expected to stay constant until 90° . However, in this study, a linear approximation is used under a pole pitch (see Figure 4) and the magnet span effect is neglected. As seen in Figure 4, this assumption is reasonable. As the performance calculation results prove, this approximation does not affect the accuracy of predictions. Length of these 10 sections is equal and MMF can be calculated using equation (7), where H_i is the field intensity, ΔL_i is the length of a given section.

$$MMF\ drop\ on\ stator\ back\ core = \sum_{i=1}^{10} (H_i \times \Delta L_i) = \Delta L_i \times \sum_{i=1}^{10} H_i \quad (7)$$

As discussed above, due to saturation in stator back-core, some of the pole flux completes its path in the air, outside the motor frame. This phenomenon is modeled by considering an air area outside of the stator by the outer diameter of diameter of $D_{o,air} = 300 \text{ mm}$ ($\approx 2.94 \times D_{o,stator}$) which is depicted in Figure 1a. In this study, diameter of the air region is selected so that at the boundary the flux density is 1% of the maximum stator back core flux density. Appendix 1 presents an analytical method for the calculation of diameter of this boundary. Significance of including the flux leaking out of the stator core and its effects on magnet operating point and performance calculation of the PMDC motor are discussed in Appendix 2.

With the above consideration, the maximum stator back core flux density $B_{s,max}$ for a given magnet flux density B_m can be determined using (8).

$$\varphi_{stator,max} = \frac{\varphi_{magnet}}{2} - \varphi_{air} \rightarrow B_{s,max} = \frac{1}{A_s} \left[\frac{A_m}{2} B_m - \frac{\sum_{i=1}^{10} (H_i \times \Delta L_i)}{\mathfrak{R}_{air}} \right] \quad (8)$$

Using the approach described above the load line for the magnetic circuit i.e B_m versus MMF drop along the magnetic circuit can be obtained. The intersection of the load line with the MMF versus B_m characteristics of the magnet ($MMF = B_m h_m$ where h_m is the magnet thickness), as seen in Figure 4b, is the operating point of the magnet. Note that given B_m , the mean air gap flux density B_{av} and hence the emf induced at this operating point can be calculated from (1).

In the sections above an analytical approach for the calculation of parameters of equivalent circuit of a brushed permanent-magnet DC motor is described. In the following sections, the accuracy of prediction of the performance of the motor using this equivalent circuit will be tested by comparing its predictions with tests performed on a test motor. Also, the results of the predictions from the analytical approach will be compared with FEM solution performance predictions.

4. The test motor

A commercial permanent-magnet brushed DC test motor is used to verify the accuracy of the approach developed in this paper. This motor is used to drive the radiator fan in automotive applications. Cross-section of this motor (4-pole, 225 W, 26 V), is depicted in Figure 1. Rotor structure and winding configuration can also be seen in Figure 1b. Lap winding is used in the armature with 60 conductors per slot. There are 4 parallel paths in the winding. The specifications of the test machine are given in Appendix 2.

The armature resistance is measured by applying a voltage to the motor terminals and measuring the current. The coil resistance is calculated in the usual manner, and considering that the brush short circuits two laminations, the resistance that appears across the brushes is calculated. The coil resistance is subtracted from measured armature resistance and the difference is assumed to be the brush resistance, which is given in Appendix 2. The brush drop nonlinearity and its dependence on the temperature is neglected in this paper.

5. Verification of the proposed analytical model

In the verification process, the applied voltage to the motor is set to 26 V, which is the rated voltage of the test machine. In analytical predictions, copper loss calculation is easy as the armature current is available. In the prediction of losses, a simple approach is used. Since the armature magnetic material flux densities are available from the method, W/kg loss curves of the magnetic material is used in the usual manner.

For verification purposes, first, the open-circuit characteristic of the test motor is predicted using the method described in this paper. The open-circuit characteristics of the motor is also measured by driving it at various speeds. Measured and predicted open circuit characteristics of the test motor are given in Figure 6. It can be observed from Figure 6 that the open-circuit characteristics of the machine is well predicted by the proposed method.

Next, the operating point of the magnet and consequently the flux densities in different parts of the motor are calculated using the proposed analytical model. The test motor is also simulated using 3-D FEM. In this solution, the number of meshes is selected automatically as 35216 by the software, and transient solver is used to carrying out the simulations. The motor circuit model for two commutator segments is shown in Figure 5. The resistance values in Figure 5 are set to half of one coil resistance (see Appendix 2) because a half symmetric model is used in simulations.

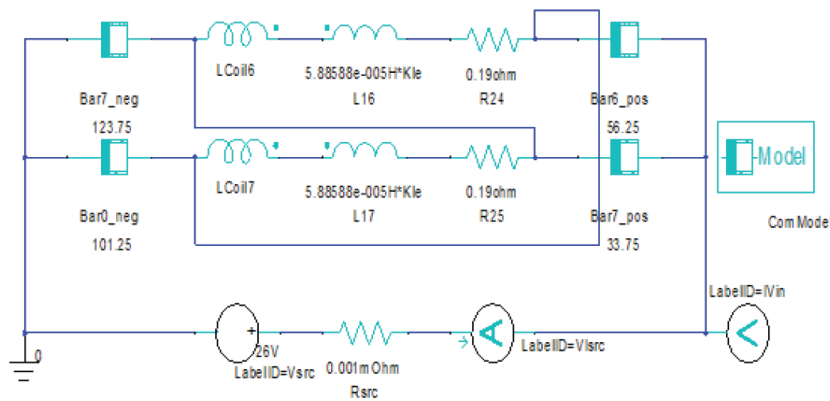


Figure 5. PMDC motor excitation circuit for two commutator segments.

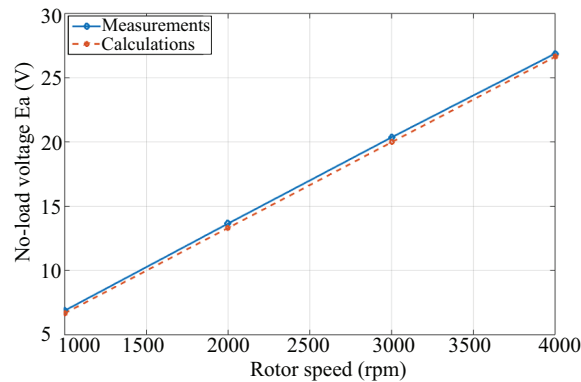


Figure 6. Predicted and measured no-load voltage vs speed.

The finite element solution indicates that the maximum stator back-core flux density is 2.25 T as given in Table 1. Variation of the stator back core flux density variation is given in Figure 4. Based on the B-H characteristic of the stator and rotor core, the knee point of the curve happens approximately at $B = 1.8$ T. So, it can be concluded that the stator back-core goes into heavy saturation in this application.

Although the higher flux density on the stator side does not cause any core loss since the stator flux is DC, it leads to a huge MMF-drop on the stator back-core and decreases the magnet flux density. Consequently,

the pole flux decreases significantly. As a consequence, the efficiency of the motor is reduced. This large MMF drop on stator back-core can be reduced by increasing the stator frame thickness or stator length.

The steady-state performance (torque, speed, input current, and losses) of the test motor is predicted motor at full load and at rated speed, using the proposed analytical method and presented in Table 2. Table 2 also includes the performance calculations for the test motor obtained using FE simulations and measurements (First 3 rows of the table). This table shows that the analytical calculation method proposed has very good accuracy and the prediction accuracy is just as good as FEM predictions. Predicted torque, output power, and efficiency of the motor are within a few percent of the measured values.

Predicted flux density values in various parts of the test motor are already presented in Table 1. In this table, FEM calculated values are also given. As can be observed from the table flux density prediction accuracy of the analytical method is very good too.

The test motor performance is also predicted under 60% and 80% of the nominal load in Table 3 and Table 4, respectively. In these tables measurement results and 3-D finite element simulation results for the same operating conditions are presented. It can be observed that analytically calculated results are in very good agreement with 3-D FE simulations and experimental results.

By comparing the analytically predicted open-circuit characteristics and underload performance of the test motor, as well as the flux density calculation results, with measurements and 3-D finite element simulations, the excellent accuracy of the proposed analytical model is verified.

Table 2. Performance calculations of test motor at full load using both FEM and analytical simulations with and without considering the outer air region.

Parameter		Speed (rpm)	Torque (N.m)	Input current (A)	Input power (W)	Output power (W)	Core loss (W)	Copper loss (W)	$P_{f\&w}$ (W)	Total losses (W)	η (%)
Considering the outer air region	Analytical	2761	0.825	13.57	352.82	227.83	13.07	101.22	10.7	124.99	64.57
	FEM	2761	0.833	13.75	357.5	230.15	14.8	101.85	10.7	127.35	64.38
	Measured	2761	0.825	13.85	360.05	227.77	13.4	108.18	10.7	132.28	63.3
Without considering the outer air region	Analytical	2761	0.88	15.52	403.52	243.74	12.31	133.57	10.7	159.78	60.4
	FEM	2761	0.89	15.49	402.74	246.63	11.9	134.51	10.7	156.11	61.24
Difference between measurements and FE results with considering the outer air region (%)		0	0.97	-0.72	-0.71	1.04	9.93	5.85	0	-3.73	1.71
Difference between measurements and FE results without considering the outer air region (%)		0	7.88	11.84	11.86	8.28	-11.72	24.34	0	15.01	-3.25
Percentage of accuracy improvement		0	6.91	11.12	11.15	7.24	1.79	18.49	0	14.28	1.54

To illustrate the importance of developing a model, which includes the flux leaking out of the magnetic circuit, Table 1 and Table 2 present the flux density and performance prediction of the test motor when the outer air region is not included in the model.

Table 1 illustrates that including the outer air region in the model changes the magnet operating point and increases the flux density in the air gap, the rotor teeth, and the stator back core by 4.5%, 7.8%, 12.9%, and 7.2%, respectively.

The performance of the test motor with and without the outer air region are presented under full load condition in Table 2, When this table is investigated, it can be observed that when the outer air region is

Table 3. Performance calculations of test motor at 60% of full load using both FEM and analytical simulations.

Parameter	Speed (rpm)	Torque (N.m)	Input current (A)	Input power (W)	Output power (W)	Core loss (W)	Copper loss (W)	Total losses (W)	$P_{f\&w}$ (W)	η (%)
Analytical	3231	0.486	8.33	230.4	151.9	21.6	44.4	12.52	78.5	65.9
FEM	3231	0.47	7.97	207.2	139.2	16.8	40.7	12.52	70.02	67.1
Measured	3231	0.433	8	208.2	133.9	20.81	40.97	12.52	74.3	64.3

Table 4. Performance calculations of test motor at 80% of full load using both FEM and analytical simulations.

Parameter	Speed (rpm)	Torque (N.m)	Input current (A)	Input power (W)	Output power (W)	Core loss (W)	Copper loss (W)	Total losses (W)	$P_{f\&w}$ (W)	η (%)
Analytical	2995	0.658	11.13	289.38	194.76	13.64	69.37	11.61	94.62	67.3
FEM	2995	0.65	10.92	284.5	192.5	13.61	66.78	11.61	92	67.7
Measured	2995	0.624	10.93	284.51	184.53	21.47	66.9	11.61	99.98	64.9

considered, prediction results are in much better agreement with the measurements. Torque, input current, and efficiency prediction accuracy improves by about 6.91%, 11.12%, and 1.54%, respectively. These results clearly illustrate how important it is to consider the flux leaking out of the stator when back-core is saturated.

6. Conclusion

In this paper, an accurate analytical model is proposed for brushed PMDC motors, which can be used for performance prediction and optimization of brushed permanent magnet DC motors. The proposed analytical method is capable of calculating no-load and underload characteristics of the machine while taking the nonlinearities of the magnetic circuit and saturation effects into account.

A calculation method using Carter's coefficient is introduced to determine the effective length of the magnet in PM motors. Moreover, the effect of flux passing through the surrounding air due to heavy saturation conditions is also taken into account by defining an air region outside of the stator. The equivalent magnetic circuit of the motor is modified accordingly.

Finally, flux density distribution, no-load, and underload performance of the test motor is predicted using the proposed analytical method. The accuracy of the proposed method is shown to be excellent by comparing analytically calculated results with measurements and finite element simulations. With these properties, the proposed model is an excellent tool for mathematical design optimization in industrial applications.

This statement can be better explained when it is recalled that in the optimization process, the performance of the motor optimized is called at each iteration. If genetic optimization is used, as done by the authors, it is found that the performance of the motor is called nearly thousand times. When the performance of the motor is calculated from the analytical approach presented here, this calculation takes about a second. The same performance at a given speed can be only calculated via FEM transient solution (2-D) and takes about 1800 s. Therefore, the computational burden is immensely increased.

The optimization of the test motor is performed by the authors. This motor is manufactured and tested as well. This process is planned to be the subject of a future paper.

Acknowledgment

This research has been funded by FAZ A.Ş, İzmir, Turkey.

References

- [1] Ackva A, Ombach G, Junak J. Numerical coupled analysis of DC motors including saturation and commutation effects. *Power Electronics and Applications* 2005; 1 (1): P1-P6. doi: 10.1109/EPE.2005.219267
- [2] Aker MN, Lu TF, Li Q. Weight optimisation of brush-type wound-field direct current motors. In: *Proceedings of the IEEE Internatinal Symposium on Intelligent Control*; Vancouver, BC, Canada; 2002. pp. 397-402.
- [3] Aker MN, Lu TF. A method for optimising the weight and response of brush-type wound-field direct current motors. In: *7th International Conference on Control, Automation, Robotics and Vision, 2002. ICARCV 2002*; Singapore; 2002. pp. 1343-1348.
- [4] Wang S, Hong J, Sun Y, Cao H. Effect Comparison of Zigzag Skew PM Pole and Straight Skew Slot for Vibration Mitigation of PM Brush DC Motors. *IEEE Transactions on Industrial Electronics* 2020; 67 (1): 4752-4761. doi: 10.1109/TIE.2019.2927175
- [5] Hunstable FE. Brushed electric motor/generator 2019; US Patent 10,284,029.
- [6] Klein FN, Kenyon ME. Permanent magnet DC motors design criteria and operation advantages. *IEEE Transactions on Industry Applications* 1984; IA-20 (6): 1525-1531. doi: 10.1109/TIA.1984.4504637
- [7] Cros J, Viarouge P, Kakhki MT. Design and optimization of soft magnetic composite machines with finite element methods. *IEEE Transactions on Magnetics* 2011; 47 (10): 4384-4390. doi: 10.1109/TMAG.2011.2157113
- [8] Yamazaki K, Kanou Y. Shape optimization of rotating machines using time-stepping adaptive finite element method. *IEEE Transactions on Magnetics* 2010; 46 (8): 3113-3116. doi: 10.1109/TMAG.2010.2043651
- [9] Tarvirdilu-Asl R. Optimum pole combination to maximize torque density in switched reluctance motors for electric vehicle applications. M.Sc, Middle East Technical University, Ankara, Turkey, 2016.
- [10] Tarvirdilu-Asl R, Zeinali R, Ertan HB. FEM-based design modifications and efficiency improvements of a brushed permanent magnet DC motor. In: *2017 International Conference on Optimization of Electrical and Electronic Equipment (OPTIM) & 2017 Int Aegean Conference on Electrical Machines and Power Electronics (ACEMP)*; Braşov, Romania; 2017. pp. 401-407.
- [11] Zhu ZQ, Jewell GW, Howe D. Finite element analysis in the design of permanent magnet machines. In: *IEE Seminar on Current Trends in the Use of Finite Elements (FE) in Electromechanical Design and Analysis (Ref. No. 2000/013)*; London, UK; 2000. pp. 1/1-1/7.
- [12] Hayashi Y, Mitarai H, Honkura Y. Development of a DC brush motor with 50% weight and volume reduction using an Nd-Fe-B anisotropic bonded magnet. *IEEE transactions on magnetics* 2003; 39 (1): 2893-2895. doi: 10.1109/TMAG.2003.815739
- [13] Boglietti A, Cavagnino A, Tenconi A. Low cost solutions to reduce cogging torque and acoustic noise of small brushed DC motors for automotive radiator cooling fan modules. In: *IECON 2012 - 38th Annual Conference on IEEE Industrial Electronics Society*; Montreal, QC, Canada; 2012. pp. 1870-1876.
- [14] Boules N. Design optimization of permanent magnet DC motors. *IEEE Transactions on Industry Applications* 1990; 26 (4): 786-792. doi: 10.1109/28.56006
- [15] Cros J, Sincero GCR, Viarouge P. Design method for brush permanent magnet DC motors. In: *2009 IEEE International Electric Machines and Drives Conference*; Miami, FL, USA; 2009. pp. 1625-1632.
- [16] Zaki A, Ibrahim S. Modeling and analysis of PM brushed DC motor using FEM. In: *2005 European Conference on Power Electronics and Applications*; Dresden, Germany; 2005. pp. P1-P6.

- [17] Abeykoon AMHS, Senevirathne HR. Disturbance observer based current controller for a brushed DC motor. In: 2012 IEEE 6th International Conference on Information and Automation for Sustainability; Beijing, China; 2012. pp. 47-52.
- [18] Acarnley PP, Al-Tayie JK. Estimation of speed and armature temperature in a brushed DC drive using the extended Kalman filter. *Electric Power Applications* 1997; 144 (1): 13-20. doi: 10.1049/ip-epa:19970927
- [19] Kumar CA, Nair NK. Multi-objective PI controller design with an application to speed control of permanent magnet DC motor drives. In: 2011 International Conference on Signal Processing, Communication, Computing and Networking Technologies; Thuckafay, India; 2011. pp. 424-429.
- [20] Santana J, Naredo JL, Sandoval F, Grout I, Argueta OJ. Simulation and construction of a speed control for a DC series motor. *Mechatronics* 2002; 12 (1): 1145-1156. doi: 10.1016/S0957-4158(02)00019-3
- [21] Scott J, McLeish J, Round WH. Speed control with low armature loss for very small sensorless brushed DC motors. *IEEE Transactions on industrial electronics* 2009; 56 (4): 1223-1229. doi: 10.1109/TIE.2008.2007046
- [22] Yildiz AB. Electrical equivalent circuit based modeling and analysis of direct current motors. *International Journal of Electrical Power & Energy Systems* 2012; 43 (1): 1043-1047. doi: 10.1016/j.ijepes.2012.06.063
- [23] Glowacz Z, Glowacz W. Mathematical model of DC motor for analysis of commutation processes. In: 2007 IEEE International Symposium on Diagnostics for Electric Machines, Power Electronics and Drives; Craców, Poland; 2007. pp. 138-141.
- [24] Martínez JSV, López PG, Juárez JJM. Series Wound DC Motor modeling and simulation, considering magnetic, mechanical and electric power losses. In: 2009 52nd IEEE International Midwest Symposium on Circuits and Systems; Cancún, Mexico; 2009. pp. 1073-1077.
- [25] Ishak D, Hassan AHA. Analytical modeling of permanent magnet excited brushed DC motor for low-cost applications. In: 2008 5th International Symposium on Mechatronics and Its Applications; Amman, Jordan; 2008. pp. 1-5.
- [26] Dalal A, Singh AK, Kumar P. Effect of saturation on equivalent circuit analysis of induction motor in practical scenario. In: 2013 Annual IEEE India Conference (INDICON); Mumbai, India; 2013. pp. 1-5.
- [27] Guha S, Kar NC. A new method of modeling magnetic saturation in electrical machines. In: 2006 Canadian Conference on Electrical and Computer Engineering; Ottawa, Canada; 2006. pp. 1094-1097.
- [28] Moallem M, Dawson GE. An improved magnetic equivalent circuit method for predicting the characteristics of highly saturated electromagnetic devices. *IEEE Transactions on magnetics* 1998; 34 (5): 3632-3635. doi: 10.1109/20.717858
- [29] Pyrhönen J, Ruuskanen V, Nerg J, Puranen J, Jussila H. Permanent-magnet length effects in AC machines. *IEEE transactions on magnetics* 2010; 46 (10): 3783-3789. doi: 10.1109/TMAG.2010.2050002
- [30] Krause P, Wasynczuk O, Sudhoff S, Pekarek S. *Analysis of electric machinery and drive systems*. Hoboken, NJ, USA: Wiley-IEEE Press, 2002.
- [31] Say MG. *Alternating current machines*. New York, USA: Pitman, 1976.
- [32] Miller TJE. *Brushless permanent Magnet and reluctance motor drives*. Oxford, UK: Oxford Science Publications, 1989.

Appendix

Appendix 1: Determination of the boundary of FE Solution

Assume that the boundary of FE solution is to be placed so that the change in the flux density at the boundary will be less than 1% of the highest back core flux density. Consider Figure 7. Imagine that layers of rings with the same width as the stator back iron width ($h_{bc, \text{stator}}$) are placed around the stator. If the mean diameter of a ring is D_i , the ring flux crosses an area given by

$$A_i = h_{bc, \text{stator}} L_{\text{stator}} \quad (9)$$

Where L_{stator} is the length of the stator core. In that case, the reluctance of the i^{th} ring can be approximated by

$$\mathfrak{R}_i = \frac{\pi D_i}{p \mu_o A_i} \quad (10)$$

If there are n rings, the reluctance of the n^{th} ring will be

$$\mathfrak{R}_i = \frac{\pi D_i}{p \mu_o A_n} \quad (11)$$

Suppose that the flux density of the stator back core is B_{bc} . In that case, flux in the stator iron core is

$$\varphi_{bc} = B_{bc} A_{bc} \quad (12)$$

Since we wish to have 1% of φ_{bc} in the boundary ring, it is easy to conclude that the reluctance of the outer ring is approximately

$$\mathfrak{R}_n = 100 \mathfrak{R}_{bc} = \frac{100 \pi D_{bc}}{p \mu_{bc} A_i} \quad (13)$$

μ_{bc} is the permeability of stator iron at B_{bc} . Therefore,

$$D_n = \frac{100 D_{bc}}{\mu_{bc}} \quad (14)$$

For the stator back core flux density of $B_{bc} = 2.25$ T, we have $H_{bc} = 52107$ A/m. Therefore, $\mu_{bc} = \mu_0 \mu_r = 4.318 \times 10^{-5}$. By substituting the parameters of the machine into equation (14), the mean outer diameter is found as 0.29 m, which is almost the same value found from FE simulations (0.3 m).

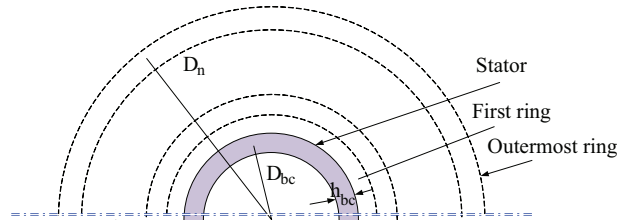


Figure 7. Determination of outer boundary for field solution.

Appendix 2: Test motor data

26 V, 4-pole, 225 W, Armature lap winding

30 turns per coil, wire diameter of 0.5 mm

Number of parallel paths, $a = 4$

Coil end extension length $L_{end} = 40$ mm

End connection length of the coil to commutator bars, $L_{wc} = 40$ mm

Brush resistance = 0.275 Ω

Coil resistance = 0.38 Ω

Stator outer diameter = 102 mm

Stator inner diameter = 81.93 mm

Rotor core length = 22.7 mm

Magnet length = 39 mm

Stator core length = 44 mm

Appendix 3: Core material data

Magnetization data of the test motor core material					
Row	B(mT)	H(A/m)	Row	B(mT)	H(A/m)
1	101.6575	48.07692	8	1510.497	877.4038
2	350.2762	72.11538	9	1620.994	2283.654
3	571.2707	96.15385	10	1731.492	5468.75
4	792.2652	120.1923	11	1841.989	10456.73
5	902.762	132.2115	12	1897.238	14002.4
6	1123.757	180.2885	13	2007.735	25180.29
7	1455.249	637.0192			